Boehmite Nanofiber–Polymethylsilsesquioxane Composite Aerogels: Synthesis, Analysis, and Thermal Conductivity Control via Compression Processing

Gen Hayase*

Frontier Research Institute for Interdisciplinary Sciences, Tohoku University, 6-3 Aramaki-aza Aoba, Aoba-ku, Sendai 980-8578, Japan

*Corresponding author: E-mail address: gen@aerogel.jp

Present addresses: International Center for Materials Nanoarchitectonics, National Institute for Materials Science, 1-1 Namiki Tsukuba, Ibaraki 305-0044 Japan

Abstract

Tri-functional organosilicon alkoxide, methyltrimethoxysilane (MTMS), was added to a boehmite nanofibers aqueous dispersion, the colloidal nanofibers were coated and bonded with polymethylsilsesquioxane (PMSQ), to produce transparent to translucent wet gel monoliths. Low bulk density composite aerogel panels were prepared by CO_2 supercritical drying of the wet gel monoliths before their mechanical properties, and thermal conductivity were investigated. As the amount of the MTMS in the starting composition increased, the fibrillar monolith skeleton coated with PMSQ thickened. Correspondingly, the Young's modulus of the monoliths increased, and the thermal conductivity decreased. When the amount of MTMS added was small, it was possible to deform the translucent panels by uniaxial compression. After 30 % uniaxial compression of the panel, the thermal conductivity was suppressed by 19 %. The thermal conductivity response to compressive deformation of fibrous aerogels, after fabrication, may inform future insulation material development.

Keywords

sol–gel; aerogels; nanofibers; thermal insulation; macroporous monoliths; composites

1. Introduction

Nanomaterial researchers have developed nanofibers with various compositions that have high mechanical properties, as one-dimensional materials, and have been applied as high-performance separation filters and fillers for resins.[1-6] Recently, three-dimensional microstructures with a cotton-like morphology have been devised for used in monolithic applications such as electrode

materials for Li-ion batteries, which require a large specific surface area.[7, 8] Although this material's wide dissemination is cost-prohibitive, compared to conventional fibrous materials, it is a research material with potential. A typical example of a conventional fibrous ceramic material is asbestos. This inexpensive and easy-to-process material had been widely used as an insulator, insulator, and friction material because of its excellent processability (spray painting and compression molding), heat resistance, insulation, and heat retention properties. However, due to the health risks posed by asbestos particulate ingestion and inhalation, its use has been prohibited. It is believed that one-dimensional ceramic materials, used under safe conditions with no shattering, will produce excellent application materials; thus, research into alternative materials for asbestos is still underway. If nanofiber materials can be successfully substituted, the application of these materials will significantly expand.

The oxide and hydroxide composites of titanium and aluminum have been extensively studied as one-dimensional nanoceramic materials.[9-13] Several have been prepared in the liquid phase and assembled into monoliths that can be used as separation media and catalyst carriers.[14, 15] We are working with nanofibers of aluminum oxide hydroxide (boehmite, AlOOH), which was reported by Nagai et al.[16] These boehmite nanofibers (BNFs) are stable and dispersible in weak acidic aqueous solutions for more than a few months, but instantly gel when the pH rises. We have succeeded in preparing highly transparent, ultralow bulk density aerogel/cryogel structures by supercritical drying/vacuum lyophilization of wet gels obtained by pH change.[17-19] Kodaira et al. have prepared a unique porous insulating material, that is reflective over a wide range of wavelengths, by evaporative drying with appropriate control of the aggregation of BNFs.[16, 20]

While monolithic materials with various bulk properties formed from stable dispersions of other nanofiber material compositions have not been reported, porous materials, based on BNFs,

still present many challenges and scope for development. The dried BNF materials are susceptible to water and moisture. Also, to maintain the dispersibility of the colloid, the density of nanofibers in the starting solution is kept low to prevent agglomeration. There is, therefore, a problem of low skeletal density when attempting to obtain a uniform gel. Although typical ultralow bulk density aerogels are relatively easy to obtain, the mechanical strength of such materials is low, and the low skeletal density results in poor insulation performance due to the free movement of gas molecules within the enlarged pores.

Our current focus is on monolithic porous materials consisting of nanofibrous composite skeletons. It has been reported that monoliths can be prepared by physically coating colloidal particles, dispersed in a liquid, with polymers and bonding them together during a sol–gel process.[21, 22] We also found that similar bulk materials can be prepared by using (pseudo)boehmite nanomaterials in a colloid.[23, 24] In a previous study, this method was applied to BNF-polymethylsilsesquioxane (PMSQ, $CH_3SiO_{1.5}$) compositions and reported to fabricate monolithic porous materials with a high Young's modulus concerning the bulk density. Also, the potential application of vacuum insulation as a core material was demonstrated. In this study, we attempted to produce composites with limited Young's modulus and compressible deformation by reviewing the composition and process. Various aerogels were prepared according to the content of PMSQ and evaluated for changes in properties.

2. Experimental

2.1. Materials

Methyltrimethoxysilane (MTMS, $CH_3Si(OCH_3)_3$), a PMSQ precursor, was purchased from Tokyo Chemical Industry Co., Ltd. (Japan). BNF acetic acid aqueous dispersion F1000 (7.2 wt %

in 2 M acetic acid aqueous solution) was kindly provided by Kawaken Fine Chemicals Co., Ltd. (Japan). Methanol, 2-propanol, and hexamethylenetetramine were obtained from Wako Pure Chemical Industries, Ltd. (Japan). All reagents were used as received.

2.2. Sample Preparation

To prepare the BNF–PMSQ composite monoliths, x mL of MTMS was first added to 200 mL of 20-fold diluted BNF dispersion (0.36 wt % in acetic acid aqueous solution), and the mixture was stirred for 10 min. After ultrasonic deaeration, the mixture was poured into, then sealed, in a container for gelation at 40 °C, which took several hours. After 2 d of incubation at 40 °C, the wet gel was washed with methanol, and the solvent was replaced with 2-propanol. Finally, BNF–PMSQ aerogel samples were obtained by CO_2 supercritical drying under 14 MPa at 80 °C. The aerogel samples obtained are referred to, hereafter, as A*x*, where *x* denotes the volume (mL) of MTMS added to 200 mL of the BNF dispersion. To prepare the xerogel samples X200 (*x*=200), evaporative drying was performed at room temperature (RT) over 12 h in a container designed to gradually diffuse 2-propanol vapor. Other attempts to obtain aerogel/xerogel samples at *x*=50, 75, 100, and 150 were not reproducible.

The pure BNF aerogel was prepared as previously described.[17] Hexamethylenetetramine (7.5 g) was added to 150 mL of diluted BNF solution and kept for 12 h at 80 °C. During this time, the solution gelled due to an increase in pH. The wet gel was then washed with methanol and 2-propanol and supercritically dried.

2.3. Characterization

The microstructures were examined using scanning electron microscopy (SEM; S-5200, Hitachi High-Technologies Corp., Japan) and transmission electron microscopy (TEM; H-7650,

Hitachi High-Technologies Corp., Japan). To prepare the A10 sample for TEM observation, wet gel was crushed and evaporatively dried. For the other samples, the monoliths were impregnated with epoxy resin and then sectioned by a microtome. The bulk densities were calculated based on the respective measured weights and volumes with an error-margin within approximately 5 %.

Nitrogen adsorption measurements, at 77 K, using BELSORP-mini II (MicrotracBEL Corp., Japan), were performed to calculate specific surface areas by applying the BET method. Samples were degassed under vacuum at 80 °C for 8 h before each measurement. Uniaxial compression tests were performed using a universal/tensile tester (EZ-SX, Shimadzu Corp., Japan) and a 100 N pressure gauge. Cylindrical samples with a diameter and height of approximately 18 mm and 7 mm, respectively, were used for the compression test. The Young's modulus was calculated from stress changes under compressive strains ranging from 2.5 % to 5.0 %.

The visible light transmittance was measured using a spectrophotometer (HSU-100H, Asahi Spectra Co., Ltd., Japan) equipped with a halogen light source (HL-20, Asahi Spectra Co., Ltd., Japan) and an integrating sphere (HSU-O-DTR, Asahi Spectra Co., Ltd., Japan). The direct-hemispherical transmittance was recorded, and the transmittance data obtained at 550 nm were normalized to a thickness of 10 mm using the Lambert–Beer equation. The thermal conductivity was measured at 25 °C using a heat flow meter (HFM 436 Lambda and HFM 446 Lambda Small, Netzsch GmbH, Germany), of aerogel panels with a size of 110 mm × 105 mm × 10 mm. For A10, samples were also prepared between two parallel PTFE plates and spacers and compressed to 7, 8, and 9 mm thick. Thermogravimetric–differential thermal analysis (TG–DTA) was performed with Thermo plus TG 8120 (Rigaku Corp., Japan) instrument at a heating rate of 10 °C min^{-1} with supplying air rate of 100 mL min^{-1}.

3. Results and Discussion

3.1. Preparation of BNF–PMSQ composite aerogels and their structural and mechanical properties

As previously reported, the dilute BNF-dispersed acetic acid aqueous solutions were gelled by the addition of MTMS, which formed a PMSQ layer on the nanofiber surface. Subsequent supercritical drying produced BNF–PMSQ aerogels with low bulk density (Figure 1). The aerogel samples prepared in this study and their respective properties are shown in Table 1. The dried aerogels prepared with low amounts of MTMS were transparent/translucent (Figure 2) but became progressively whiter/opaquer as the amounts of MTMS increased due to Mie scattering as the local scale due to the skeletal and pore structure became closer to the wavelength of visible light.[25] The increase in bulk density combined with the SEM images of each sample (Figures 3a–e and 4a,b) suggest that the PMSQ coating progressively thickened. Although transparent wet gels were obtained when the MTMS amount was low (e.g., x=5), they shrunk significantly after supercritical drying. The skeleton was unable to bear its weight due to the weak adhesion, between the nanofibers, achieved by the MTMS-derived PMSQ. For x=10 and above, aerogels were obtained with good yield. However, large A20 samples were vulnerable to cracking, and although crack-free A20 samples with an area of approximately 100 cm^2 and less were produced, a clean sample that could be used for thermal conductivity measurements (described later), was not obtained. Below x=50, the aerogel skeleton structure is fibrillar, while for x>50, droplet-like formations are observed between the fibrils (Figures 3f and 4c). The formation is due to the macroscopic phase separation (formation of sea–island structure) of some of the PMSQ without coating the nanofibers when the MTMS addition exceeds a certain amount. Evaporative drying of the wet gel with x=50 resulted in significant shrinkage of the sample, but for x=200, the xerogel sample (evaporatively

dried at ambient temperature) was comparable to the aerogel sample (supercritically dried). In the intermediate region, 50<x<200, the formation of droplet-like structures and the shrinkage of the xerogel samples was poorly reproducible. An increase in hydrophobic PMSQ content during the sol–gel reaction, in an aqueous system, improves the smoothness of the skeletal surface, resulting in the observed lower BET specific surface area for X200.

Table 1. Properties of the BNF and BNF–PMSQ aerogel/xerogel samples.

Sample	Bulk density [mg cm^{-3}]	Young's modulus [kPa]	Thermal conductivity [mW m^{-1} K^{-1}]	BET surface area [m^2 g^{-1}]
BNF aerogel	4.5	20.8	39.6	382
A10	12.4	12.2	36.8	460
A20	30.5	22.5	A	315
A30	57.6	142	33.5	263
A40	86.8	373	28.7	216
A50	124	858	26.6	214
X200	301	350	42.2	6

a Panels of the requisite size for thermal conductivity measurements could not be obtained.

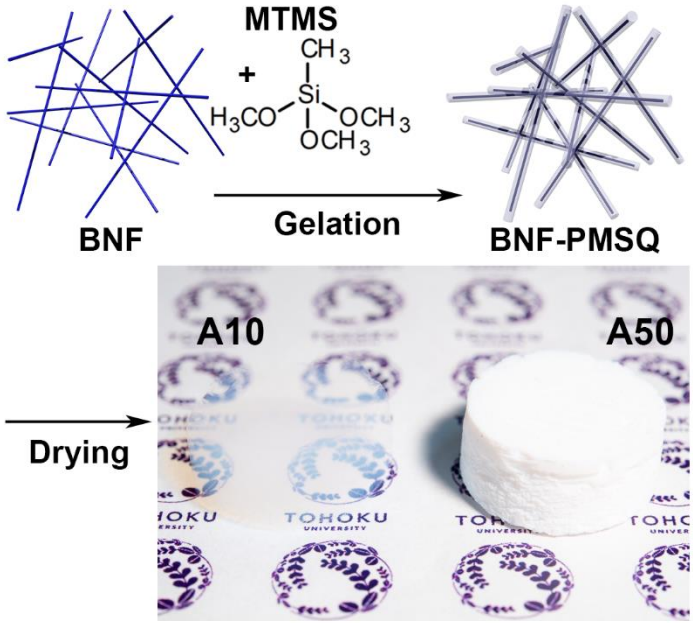

Figure 1 Schematic of the preparation of BNF–PMSQ composite monoliths and a photo of the 7 mm thick samples, the appearance of which changes from translucent to opaque depending on the amount of MTMS added.

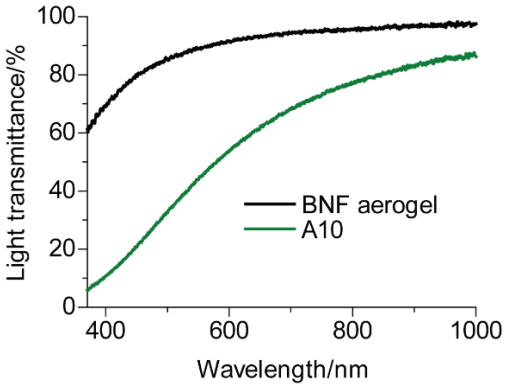

Figure 2 Visible light transmittance of BNF aerogel and A10 BNF–PMSQ aerogel (converted to 10 mm thickness using the Lambert–Beer equation); the PMSQ coating thickens the skeleton, resulting in stronger scattering of visible light.

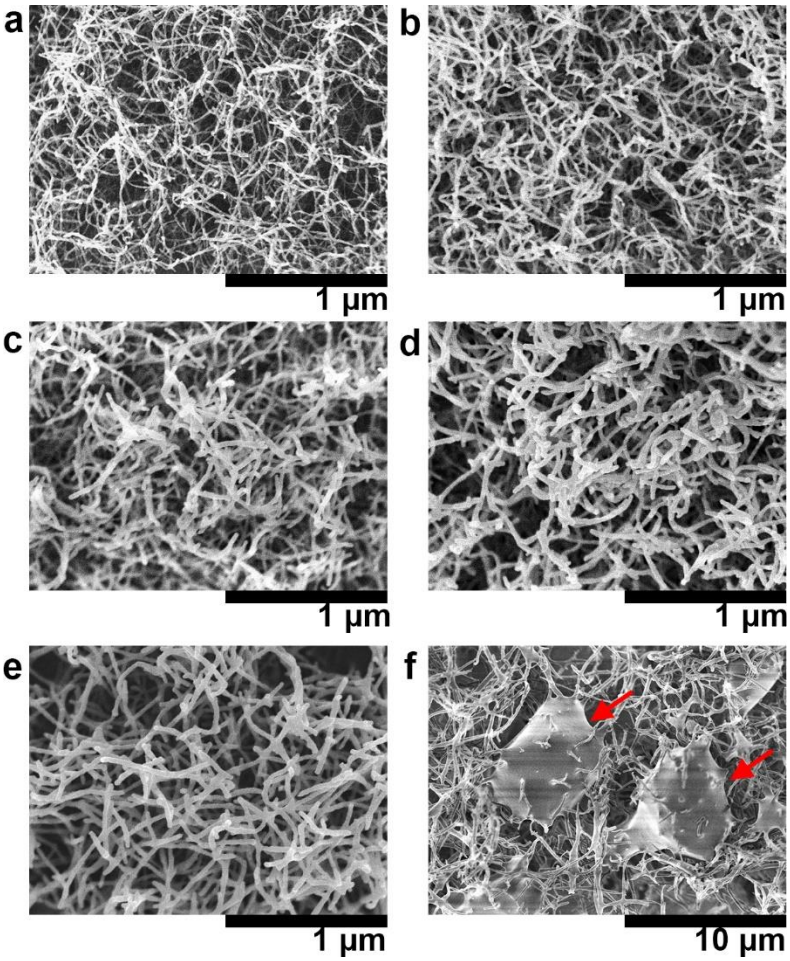

Figure 3 SEM images of BNF–PMSQ composite monoliths (a) A10, (b) A20, (c) A30, (d) A40, (e) A50, and (f) X200. The skeleton thickens with the increasing amount of MTMS added. Droplet-like formations are observed in X200 (red arrow).

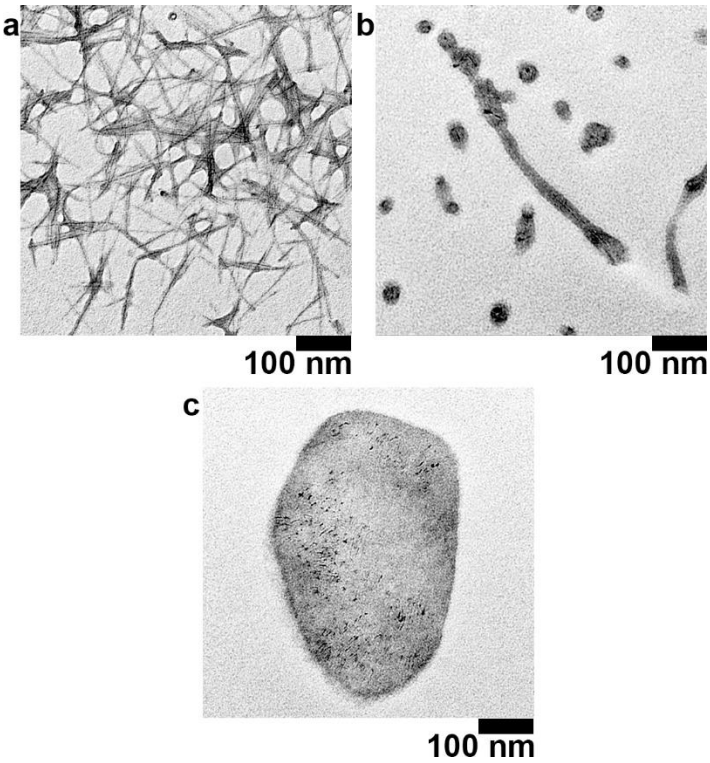

Figure 4 TEM images of the skeleton of the macroporous BNF–PMSQ composites (a) A10, (b) A50, and (c) X200. As described in the experimental section, the A10 sample was prepared by crushing the wet gel, which is different from the actual aerogel structure. However, the skeletal diameter can be compared with A50. X200 is a cross-sectional view of the droplet-like structure (see also Figure 3f), and the presence of BNF was found within.

The mechanical properties were affected by the change in the skeletal structure, depending on the amount of MTMS added. The structure of the pure BNF aerogel demonstrates low bulk density and high transmittance, but is almost irreversibly deformed by an applied external force. The structure of BNF–PMSQ uses PMSQ, generated by hydrolysis and polycondensation of MTMS, for adhesion, which increases Young's modulus and improves elasticity (Figure 5). Aerogel A10 is highly permeable and shows minimal strain recovery after uniaxial compression,

A50 shows a significant recovery, and X200 almost regains its original shape after a few dozen minutes of heating (stress relaxation). The difference in the shape of the stress–strain curves illustrate the difference in morphology. The pure BNF aerogel and A10 samples did not crack when compressed by 80 %, while the A50 sample disintegrated. As with the reports on cellulose and chitosan[26-29] it has been shown that deformation processing is possible without macroscopic separation of fibers of a material whose skeleton retains the characteristics of nanofibers.

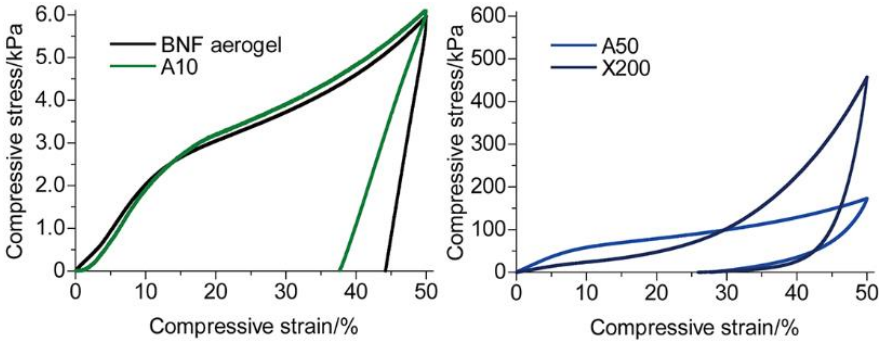

Figure 5 Stress–strain curves of BNF–PMSQ composite monoliths.

3.2. Thermal conductivity of BNF–PMSQ aerogel and its compression processed samples

The application of low-density aerogel, such as silica, as an insulation material has been extensively studied.[30-33] In this paper, the thermal conductivity of BNF–PMSQ aerogels was also measured, and the thermal insulation performance was evaluated. The thermal conductivity of a porous material is determined by three elements: solid phase, gas phase, and radiation. In the case of aerogel, in which the thermal conductivity of the gas phase is particularly important, reducing pore size, reduces the thermal momentum exchange between gas molecules within the structure.[34-37] The pure BNF aerogel has extremely low bulk density and can be regarded as having large pores since the skeletal phase occupies very little space. Accordingly, the thermal conductivity of the

BNF aerogel, attributed to the high thermal conductivity of the gas phase and the solid-phase heat transfer of the larger boehmite (compared to silica), is higher than that of previously reported silica aerogels (Figure 6a). The thermal conductivity decreased as the amount of MTMS, added to the starting composition, increased. This result is due to the low thermal conductivity of PMSQ, which physically coats the boehmite, decreasing porosity and increasing the diameter (thickening) of the skeleton which, in turn, impedes the collision of gas molecules (thermal momentum exchange). However, it is difficult to determine the average pore size change of these structures by the nitrogen adsorption measurement or mercury injection method due to the characteristics of the measurement method. Among the samples reproducibly obtained in this paper, the A50 sample demonstrated the lowest thermal conductivity at 26.6 mW m^{-1} K^{-1}. It was considered that a minimum value of thermal conductivity could be obtained by increasing the MTMS addition x, but this could not be confirmed because of the phase separation as mentioned above, which could not be reproduced.

Plappert et al. reported that thermal conductivity can be controlled, to some extent, by compressively deforming and densifying nanofiber aerogels consisting of 2,3-dicarboxyl cellulose.[29] BNF–PMSQ aerogels with low PMSQ content were tested because they could be compressively deformed without cracking (Figure 6b). When the A10 sample was uniaxially compressed by 30 %, the thermal conductivity decreased by approximately 19 %. Although no further compression could be measured, due to the size of the A10 sample (which can be made into a panel), and the measurement conditions, the results suggest that aerogel materials with a fiber-like structure can be compressed (densified) to reduce thermal conductivity. We are developing a gel specialized for such applications.

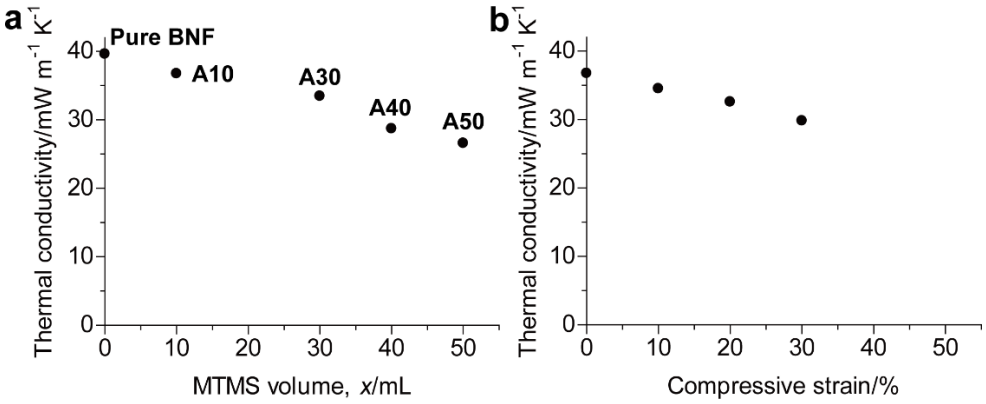

Figure 6 (a) Thermal conductivity of the BNF–PMSQ aerogels as a function of the amount of MTMS added to the starting composition. Sample A20, x=20, was prone to cracking and did not yield the panels needed for measurement. (b) Change in thermal conductivity of the A10 panel, x=10, under uniaxial compression.

The heat resistance of the A10 and A50 BNF–PMSQ aerogel samples were investigated by TG–DTA under airflow. As shown in Figure 7, the aerogel nanofibers gradually lose water vapor upon heating, and the oxidation of the methyl group of PMSQ starts at approximately 400 °C. When those samples were heated in an electric furnace, their shape were maintained in the temperature range of 350–400 °C. However, above that temperature, they started shrinking or cracking and eventually collapsed. BNF–PMSQ aerogels, which have higher heat resistance than organic and biofiber materials, have the potential to be applied as a flexible insulation material with further research and development.

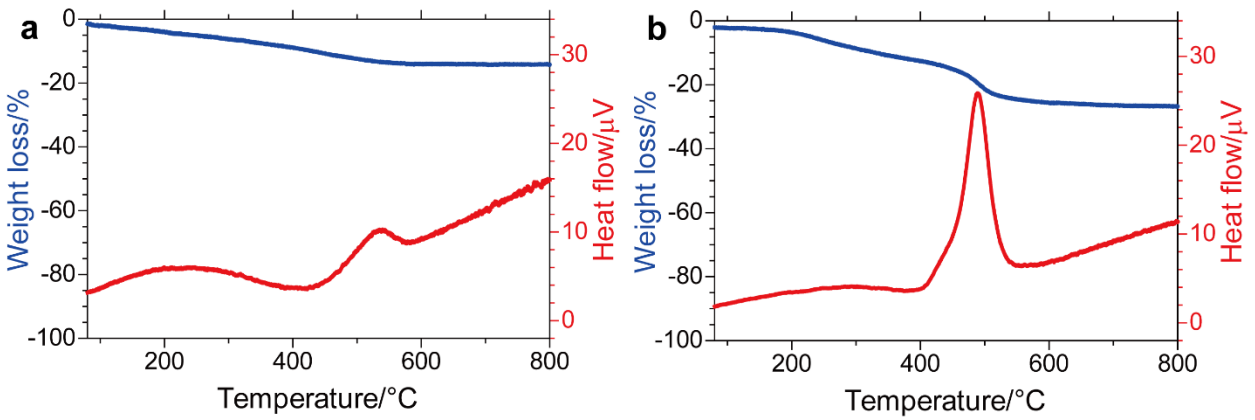

Figure 7 TG–DTA results for sample (a) A10 and (b) A50. Although dehydration occurs gradually as the temperature rises, the panels are heat resistant until the oxidation of the methyl groups occurs at approximately 350–400 °C.

4. Conclusions

Transparent to translucent wet gels were obtained by adding organosilicon alkoxide, MTMS, to dilute BNF-dispersed acetic acid aqueous solution to coat and adhere the colloidal nanofibers. These wet gels were supercritically dried to produce panel-shaped aerogel samples. A decrease in visible light transmittance and an increase in Young's modulus under uniaxial compression were observed for samples with higher PMSQ content and concomitant larger skeletal diameter. As the Young's modulus increased, the permanent compressive strain decreased. When the PMSQ composition was greatly increased, the xerogel obtained by evaporative drying showed the same physical properties as the aerogel obtained by supercritical drying, but the microstructure became inhomogeneous. As the amount of PMSQ increased, the thermal conductivity decreased because the pore size reduced due to the thickening of the skeleton structure within the monolith. Among the samples reproducibly obtained in this paper, the A50 sample demonstrated the lowest thermal

conductivity at 26.6 mW m^{-1} K^{-1}. We also succeeded in reducing the thermal conductivity of the A10 sample by 19 % by uniaxially compressing the A10 panel by 30 %. This change suggests that the thermal conductivity of the flexible nanofibril monolith can be controlled by reducing the pore size with the mechanical deformation of the sample after fabrication. We have reported to fabricate BNF aerogel-like cryogels that contain no localized aggregation structures.[18, 19] Although there are still issues to resolve, we believe that in the future, it will be possible to produce an high-performance insulation material just by compression molding of the flexible monoliths fabricated by a simpler process than conventional aerogels.

Note

The author declares no competing financial interest.

Acknowledgment

This work was supported by the Japan Society for the Promotion of Science Grants-in-Aid for Scientific Research (JSPS KAKENHI) No. 17K14541, and the Ministry of Education, Culture, Sports, Science and Technology Leading Initiative for Excellent Young Researchers (MEXT LEADER) Grant.

References

1. Lozano, K.; Barrera, E. V., Nanofiber-Reinforced Thermoplastic Composites. I. Thermoanalytical and Mechanical Analyses. *J. Appl. Polym. Sci.* **2001,** *79* (1), 125-133.
2. Hammel, E.; Tang, X.; Trampert, M.; Schmitt, T.; Mauthner, K.; Eder, A.; Potschke, P., Carbon Nanofibers for Composite Applications. *Carbon* **2004,** *42* (5-6), 1153-1158.
3. Peng, X.; Jin, J.; Ichinose, I., Mesoporous Separation Membranes of Polymer-Coated Copper Hydroxide Nanostrands. *Adv. Funct. Mater.* **2007,** *17* (11), 1849-1855.
4. Shams, M. I.; Nogi, M.; Berglund, L. A.; Yano, H., The Transparent Crab: Preparation and Nanostructural Implications for Bioinspired Optically Transparent Nanocomposites. *Soft Matter* **2012,** *8* (5), 1369-1373.
5. Samitsu, S.; Zhang, R.; Peng, X.; Krishnan, M. R.; Fujii, Y.; Ichinose, I., Flash Freezing Route to Mesoporous Polymer Nanofibre Networks. *Nat. Commun.* **2013,** *4*, 2653.
6. Deuber, F.; Mousavi, S.; Federer, L.; Hofer, M.; Adlhart, C., Exploration of Ultralight Nanofiber Aerogels as Particle Filters: Capacity and Efficiency. *ACS Appl. Mater. Interfaces* **2018,** *10* (10), 9069-9076.
7. Chen, L. F.; Zhang, X. D.; Liang, H. W.; Kong, M. G.; Guan, Q. F.; Chen, P.; Wu, Z. Y.; Yu, S. H., Synthesis of Nitrogen-Doped Porous Carbon Nanofibers as an Efficient Electrode Material for Supercapacitors. *ACS Nano* **2012,** *6* (8), 7092-7102.
8. Liang, H. W.; Wu, Z. Y.; Chen, L. F.; Li, C.; Yu, S. H., Bacterial Cellulose Derived Nitrogen-Doped Carbon Nanofiber Aerogel: An Efficient Metal-Free Oxygen Reduction Electrocatalyst for Zinc-Air Battery. *Nano Energy* **2015,** *11*, 366-376.
9. Zhu, H. Y.; Riches, J. D.; Barry, J. C., γ-alumina Nanofibers Prepared from Aluminum Hydrate with Poly(ethylene oxide) Surfactant. *Chem. Mater.* **2002,** *14* (5), 2086-2093.
10. Li, D.; Xia, Y. N., Fabrication of Titania Nanofibers by Electrospinning. *Nano Lett.* **2003,** *3* (4), 555-560.
11. Tsai, C. C.; Teng, H. S., Regulation of the Physical Characteristics of Titania Nanotube Aggregates Synthesized from Hydrothermal Treatment. *Chem. Mater.* **2004,** *16* (22), 4352-4358.

12. Yuan, Z. Y.; Su, B. L., Titanium Oxide Nanotubes, Nanofibers and Nanowires. *Colloids Surf. A* **2004,** *241* (1-3), 173-183.
13. Kuiry, S. C.; Megen, E.; Patil, S. A.; Deshpande, S. A.; Seal, S., Solution-Based Chemical Synthesis of Boehmite Nanofibers and Alumina Nanorods. *J. Phys. Chem. B* **2005,** *109* (9), 3868-3872.
14. Heiligtag, F. J.; Cheng, W.; Mendonça, V. R. d.; Süess, M. J.; Hametner, K.; Günther, D.; Ribeiro, C.; Niederberger, M., Self-Assembly of Metal and Metal Oxide Nanoparticles and Nanowires into a Macroscopic Ternary Aerogel Monolith with Tailored Photocatalytic Properties. *Chem. Mater.* **2014,** *26*, 5576-5584.
15. Okada, K.; Asakura, G.; Tokudome, Y.; Nakahira, A.; Takahashi, M., Macroporous Titanate Nanotube/TiO2 Monolith for Fast and Large-Capacity Cation Exchange. *Chem. Mater.* **2015,** *27* (5), 1885-1891.
16. Nagai, N.; Mizukami, F., Properties of Boehmite and Al_2O_3 Thin Films Prepared from Boehmite Nanofibres. *J. Mater. Chem.* **2011,** *21* (38), 14884-14889.
17. Hayase, G.; Nonomura, K.; Hasegawa, G.; Kanamori, K.; Nakanishi, K., Ultralow-Density, Transparent, Superamphiphobic Boehmite Nanofiber Aerogels and Their Alumina Derivatives. *Chem. Mater.* **2015,** *27* (1), 3-5.
18. Hayase, G., Facile Fabrication of Ultralow-Density Transparent Boehmite Nanofiber Cryogel Beads and Their Application to a Nanoglue. *ChemNanoMat* **2017,** *3* (3), 168-171.
19. Hayase, G.; Funatomi, T.; Kumagai, K., Ultralow-Bulk-Density Transparent Boehmite Nanofiber Cryogel Monoliths and Their Optical Properties for a Volumetric Three-Dimensional Display. *ACS Appl. Nano. Mater.* **2018,** *1* (1), 26-30.
20. Kodaira, T.; Suzuki, Y.-h.; Nagai, N.; Matsuda, G.; Mizukami, F., A Highly Photoreflective and Heat-Insulating Alumina Film Composed of Stacked Mesoporous Layers in Hierarchical Structure. *Adv. Mater.* **2015,** *27* (39), 5901-5905.
21. Schmidt, D. F.; von Hohenesche, C. D.; Weiss, A.; Schadler, V., Colloidal Gelation as a General Approach to the Production of Porous Materials. *Chem. Mater.* **2008,** *20* (9), 2851-2853.
22. Cingolani, A.; Cuccato, D.; Storti, G.; Morbidelli, M., Control of Pore Structure in Polymeric Monoliths Prepared from Colloidal Dispersions. *Macromol. Mater. Eng.* **2018,** *303* (1), 1700417.
23. Hayase, G.; Nonomura, K.; Kanamori, K.; Maeno, A.; Kaji, H.; Nakanishi, K., Boehmite Nanofiber-Polymethylsilsesquioxane Core-Shell Porous Monoliths for a Thermal Insulator under Low Vacuum Conditions. *Chem. Mater.* **2016,** *28* (10), 3237-3240.
24. Hayase, G., Pseudoboehmite Nanorod-Polymethylsilsesquioxane Monoliths Formed by Colloidal Gelation. *J. Asian Ceram. Soc.* **2019,** *7* (4), 469-475.
25. Mandal, C.; Donthula, S.; Soni, R.; Bertino, M.; Sotiriou-Leventis, C.; Leventis, N., Light Scattering and Haze in TMOS-co-APTES Silica Aerogels. *J. Sol-Gel Sci. Technol.* **2019,** *90* (1), 127-139.
26. Olsson, R. T.; Samir, M. A. S. A.; Salazar-Alvarez, G.; Belova, L.; Strom, V.; Berglund, L. A.; Ikkala, O.; Nogues, J.; Gedde, U. W., Making Flexible Magnetic Aerogels and Stiff Magnetic Nanopaper Using Cellulose Nanofibrils as Templates. *Nat. Nanotechnol.* **2010,** *5* (8), 584-588.
27. Takeshita, S.; Yoda, S., Chitosan Aerogels: Transparent, Flexible Thermal Insulators. *Chem. Mater.* **2015,** *27* (22), 7569-7572.

28. Zhang, J. P.; Li, B. C.; Li, L. X.; Wang, A. Q., Ultralight, Compressible and Multifunctional Carbon Aerogels Based on Natural Tubular Cellulose. *J. Mater. Chem. A* **2016,** *4* (6), 2069-2074.
29. Plappert, S. F.; Nedelec, J. M.; Rennhofer, H.; Lichtenegger, H. C.; Liebner, F. W., Strain Hardening and Pore Size Harmonization by Uniaxial Densification: A Facile Approach toward Superinsulating Aerogels from Nematic Nanofibrillated 2,3-Dicarboxyl Cellulose. *Chem. Mater.* **2017,** *29* (16), 6630-6641.
30. Rubin, M.; Lampert, C. M., Transparent Silica Aerogels for Window Insulation. *Sol. Energy Mater.* **1983,** *7* (4), 393-400.
31. Fricke, J.; Tillotson, T., Aerogels: Production, characterization, and applications. *Thin Solid Films* **1997,** *297* (1-2), 212-223.
32. Hüsing, N.; Schubert, U., Aerogels - Airy Materials: Chemistry, Structure, and Properties. *Angew. Chem. Int. Ed.* **1998,** *37* (1-2), 23-45.
33. Hrubesh, L. W., Aerogel Applications. *J. Non-Cryst. Solids* **1998,** *225* (1-3), 335-342.
34. Smith, D. M.; Maskara, A.; Boes, U., Aerogel-Based Thermal Insulation. *J. Non-Cryst. Solids* **1998,** *225* (1), 254-259.
35. Baetens, R.; Jelle, B. P.; Gustavsen, A., Aerogel Insulation for Building Applications: A State-of-the-Art Review. *Energ. Buildings* **2011,** *43* (4), 761-769.
36. Koebel, M.; Rigacci, A.; Achard, P., Aerogel-Based Thermal Superinsulation: An Overview. *J. Sol-Gel Sci. Technol.* **2012,** *63* (3), 315-339.
37. Hayase, G.; Kugimiya, K.; Ogawa, M.; Kodera, Y.; Kanamori, K.; Nakanishi, K., The Thermal Conductivity of Polymethylsilsesquioxane Aerogels and Xerogels with Varied Pore Sizes for Practical Application as Thermal Superinsulators. *J. Mater. Chem. A* **2014,** *2* (18), 6525-6531.